

Numerical Experiments on Convergence Cloud Bands over the Northern Part of the Japan Sea

By Hidetaka Sasaki and Takehiko Satomura

*Meteorological Research Institute, 1-1 Nagamine Tsukuba, Ibaraki 305, Japan
(Manuscript received 22 October 1990, in revised form 3 April 1991)*

Abstract

Two convergence cloud bands over the northern part of the Japan Sea are simulated with a 2-dimensional non-hydrostatic cloud model and the results are compared with special observations performed by the Japan Meteorological Agency. The model covers 600 km in the horizontal direction and includes Primorskii, USSR, the northern part of the Japan Sea, and Hokkaido, Japan.

We successfully simulated convergence cloud bands nearly 100 km off the west coast of Hokkaido and 70~80 km off the east coast of Primorskii. The results show that the cold air from the Asian Continent stops at the west convergence cloud band and the land breeze from the Hokkaido also stops at the east convergence cloud band.

Experiments with different lower boundary conditions and physical processes are made to examine the effects of initial wind, surface temperature, latent heat release and orography upon the convergence cloud bands. The results show that the pressure gradient induced by the gradient of the sea surface temperature causes the westerly wind between the two convergence cloud bands. Latent heat release is necessary for convection to develop fully as observed. We also find that both the sea-land temperature difference at the coast of Hokkaido and the initial wind in a lower layer are important factors in determining the position of the east convergence cloud band.

1. Introduction

Hokkaido is the northernmost district of Japan and is encircled by seas (Fig. 1). During the winter, a north-westerly monsoon wind blows from the Asian Continent and the cold air mass flowing over the Japan sea is modified from below through ample supply of heat and water vapour. Snowfall is caused by the modification of the air mass. When the north-westerly monsoon wind blows weakly, heavy snowfall of several tens of centimeters occasionally occurs in a narrow region of the west coast of Hokkaido. In most cases, a convergence cloud band and/or a meso-scale cyclone that appears off the west coast of Hokkaido participates in the heavy snowfall. The convergence cloud band is a few hundreds to one thousand kilometers in length and several tens of kilometers in width. A meso-scale cyclone whose diameter is 100~200 km occasionally appears at the south end of the convergence cloud band.

The heavy snowfall seriously affects human activities (traffic jams and house collapse by the weight of snow), and many scientists have studied the associated meteorological mechanisms and structures.

Saito *et al.* (1968) observed meso-scale cyclones using radar and suggested that the convergence of warm and wet air brought about the heavy snowfall. They, however, did not mention the dynamical structure of the meso-scale cyclones or convergence cloud band. Okabayashi (1969a, 1969b) and Okabayashi and Satomi (1971) examined satellite cloud images and composed a model of the structure of the convergence cloud band. They found that the westerly monsoon wind and a land breeze from Hokkaido formed a discontinuity line and small disturbances moved along it from north to south. Muramatsu *et al.* (1975) classified the meso-scale cyclones into two types based on the locations of synoptic-scale cyclones over Chishima-Kamchatska area and discussed their structures. Fujiyoshi *et al.* (1988) and Tsuboki *et al.* (1989) investigated the kinematical structures of convergence cloud bands that occurred in Hokkaido using a Doppler radar. They found that a convergence cloud band was formed off-shore between cold air from the land and warmer air over the sea. They also found that there were Kelvin-Helmholtz waves along the upper boundary of the shear layer. These observational studies showed that the north-westerly wind and the land breeze from Hokkaido produced a convergence cloud band. A

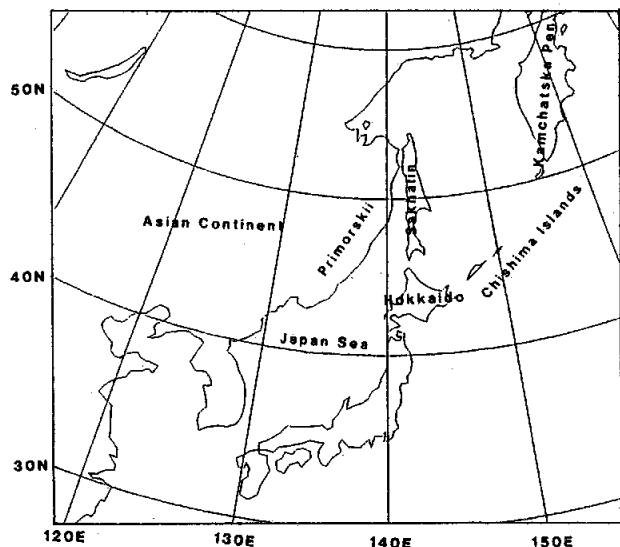


Fig. 1. Geographical map around Hokkaido.

radar observation, especially a Doppler radar on land, or a satellite can not, however, make clear the internal structure of a convergence cloud band far off the coast of Hokkaido. Therefore, the available observational data are not sufficient for comprehending the structure of a convergence cloud band.

By numerical simulation using a hydrostatic limited area model with a cumulus parameterization, Nagata and Ikawa (1988) pointed out that the difference of the temperature between the land and the sea was the most important factor forming the convergence band. The horizontal grid interval of their model (42 km) was, however, too large to see the structure of a convergence cloud band. Sasaki and Deguti (1988) applied a hydrostatic local-wind dry model to a convergence band. They discussed its structure and the factors which determined its position. They found that the velocity and the direction of the initial geostrophic wind were important factors in determining the band position and that any orographic effect was small.

The effect of latent heat release can be expected to play a significant role in the formation of a convergence cloud band, seeing that a convergence cloud band is composed of active cumulus clouds. Indeed, Ballentine (1982) and Hjelmfelt and Braham (1983) performed a numerical simulation of the convergence cloud over Lake Michigan using a hydrostatic limited area model and indicated that latent heat release played an important role in intensifying the land breeze circulation and the convergence cloud over the lake. The horizontal grid intervals of their models were about 10 km, and the method of cumulus cloud parameterization for the model whose grid intervals are about 10 km has not been established yet. Therefore, it is advisable to include the effect of cloud more accurately by treating clouds explicitly than by using the parameterization in the above

hydrostatic simulations.

Using a non-hydrostatic anelastic model with a bulk parameterization of cloud microphysics, Ikawa *et al.* (1987) examined the structure of convective snow cloud bands over the Japan Sea off the coast of the Hokuriku district. They compared the results with the observation of the snow cloud bands on 25 January 1984, and showed some agreement: multicellular structure, long lasting property, and others. They also found that the features of the snow cloud bands were similar to those of a squall line. The phenomenon treated by them is similar to ours on the point that band convection occurs over the warm sea in the winter, but their model did not include the effect of land breeze. As the above-mentioned observational studies pointed out, the land breeze is one of the important factors in the convergence cloud band formation off the west coast of Hokkaido. Hence, a model which can represent land breeze and cumulus convection explicitly is needed to simulate the convergence cloud band realistically.

The Japan Meteorological Agency (JMA) performed a special observation from 24 to 29 January 1989 for the purpose of studying the structure of convergence cloud bands and meso-scale cyclones formed off the west coast of Hokkaido. The observation and GMS (Geostationary Meteorological Satellite) images showed that two convergence cloud bands existed on 24 to 25 January: one was located about 100 km off the west coast of Hokkaido (hereafter referred to as EC; the East Convergence) and the other was located at 70~80 km off the east coast of the Asian Continent (hereafter referred to as WC; the West Convergence). Because two convergence cloud bands as in this case are seldom observed in this region, they are worth studying in detail.

In this study, we use a non-hydrostatic cloud model with elastic equations based on Satomura (1989) and study the formation mechanisms of the convergence cloud bands. We compare the results with the special observation. As cited above, the formation mechanism of a convergence cloud band was proposed by Okabayashi and Satomi (1969): a convergence cloud band is formed by convergence of the westerly monsoon wind and land breeze from Hokkaido. This formation mechanism, however, can not be applied in our case, since the convection at WC likely stops the westerly wind from Primorskii, USSR and the wind can not reach the west of EC. Thus, it is interesting to investigate the genesis and the structure of the two convergence cloud bands. We adopt a 2-dimensional numerical model to cover a wide region (from Primorskii, USSR to Hokkaido), for the model should include two convergence cloud bands.

2. Observations on 24–25 January 1989

Figure 2 is the surface synoptic map at 0900 JST

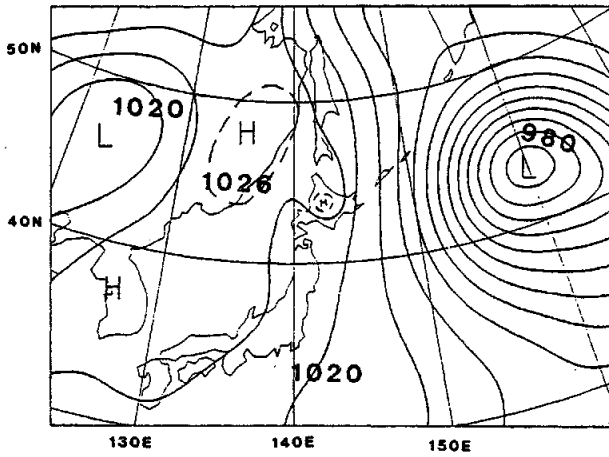


Fig. 2. Surface synoptic map at 0900 JST on 25 January 1989.

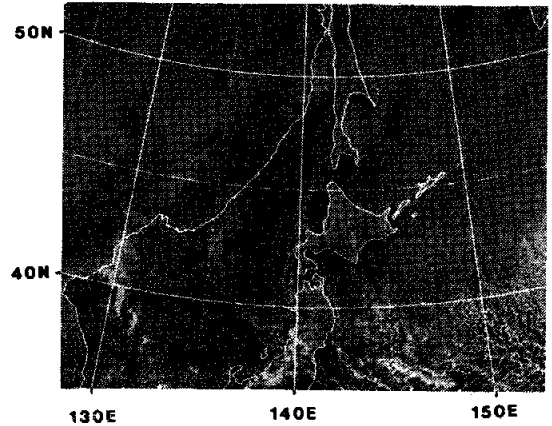


Fig. 4. Visible GMS image at 1200 JST on 25 January 1989. EC is located about 100 km off the west coast of Hokkaido and WC is located 70~80 km off the east coast of the Asian Continent.

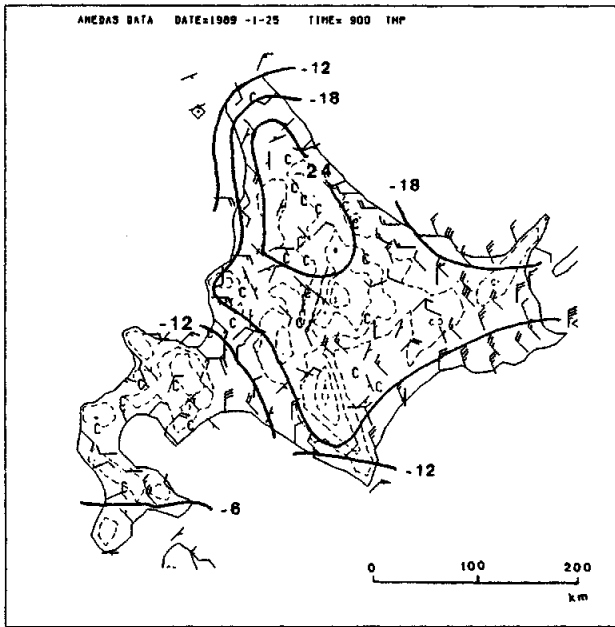


Fig. 3. Local weather chart obtained from the AMeDAS. The horizontal distribution of minimum temperature from 2100 JST on 24 to 0900 JST on 25 January. The contour interval is 6°C. Wind field is shown with C, a half barb and a full barb indicating calm, 1 m/s and 2 m/s, respectively at 0900 JST on 25 January.

(Japan Standard Time) on 25 January 1989. A developing low passed through off the Sanriku on 24 January and reached the east of Chishima Islands on 25 January. An anticyclone was identified over Primorskii, USSR, and the pressure gradient was weak in the vicinity of Hokkaido: the weather was fine and calm over the whole of Hokkaido. The horizontal distribution of minimum temperature on this morning obtained from the surface observation network named Automated Meteorological Data Acqui-

sition System (AMeDAS) is shown in Fig. 3. Because of the radiational cooling, the minimum temperature fell to about -30°C in the northern part of Hokkaido: a meso-scale anticyclone was identified and the land breeze was blowing from inland.

Figure 4 is a visible GMS cloud image at 1200 JST on 25 January. A convergence cloud band was located about 100 km off the west coast of Hokkaido and its orientation was roughly from north to south. There were almost no clouds on the east side of EC. Another convergence cloud band was located 70~80 km off Primorskii and parallel to the coast line. Convective clouds were scattered between these two convergence bands.

Figures 5a and 5b show radar echo maps observed by Keifumaru (a weather ship of the JMA) at 2100 JST on 24 and 0900 JST on 25 January, respectively. Keifumaru (point A) was located on the west side of EC and Kofumaru (another weather ship of the JMA, point B) was located on the east side of EC. According to these maps, radar echoes of a convergence cloud band appeared on the east side of Keifumaru at 2100 JST on 24 January (Fig. 5a), reached a peak intensity at 0900 JST on 25 January (Fig. 5b), and gradually decayed after that time.

Figures 6a and 6b are vertical soundings at Keifumaru and Kofumaru, respectively. The dash-dotted line in Fig. 6a shows that the relative humidity near the sea surface was 76% and gradually decreased with height up to 0.3 km at Keifumaru. It increased again up to a height of 2 km and then rapidly decreased above this level. The water vapour mixing ratio had a maximum value near the surface, gradually decreased with height up to 2 km and sharply decreased above this level. Potential temperature was almost constant up to 2 km and then increased sharply with height. Judging from the sounding, the depth of the mixed layer at Keifumaru was 2 km. On

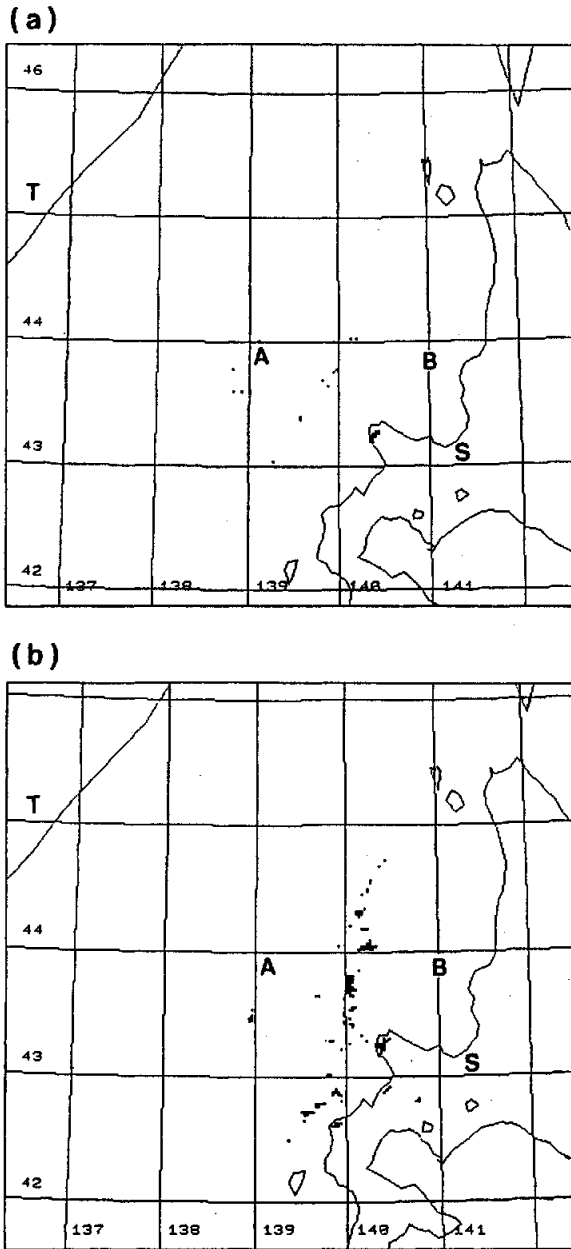


Fig. 5. Radar echo maps observed at Keifumaru. (a) 2100 JST on 24 January 1989 and (b) 0900 JST on 25 January 1989. Letters of A, B, S, T indicate the positions of Keifumaru, Kofumaru, Sapporo and Ternei, respectively.

the other hand, the sounding at Kofumaru (Fig. 6b) suggests that the depth of the mixed layer at Kofumaru was 1.2 km. The wind in the lower level of the mixed layer at Keifumaru was almost northerly and that at Kofumaru was north-easterly: there was convergence of wind between the ships.

The sea surface temperature at Keifumaru (4.9°C) was colder than that at Kofumaru (7.6°C), but the air near the sea surface at Keifumaru (-3.4°C , 76%) was warmer and wetter than that

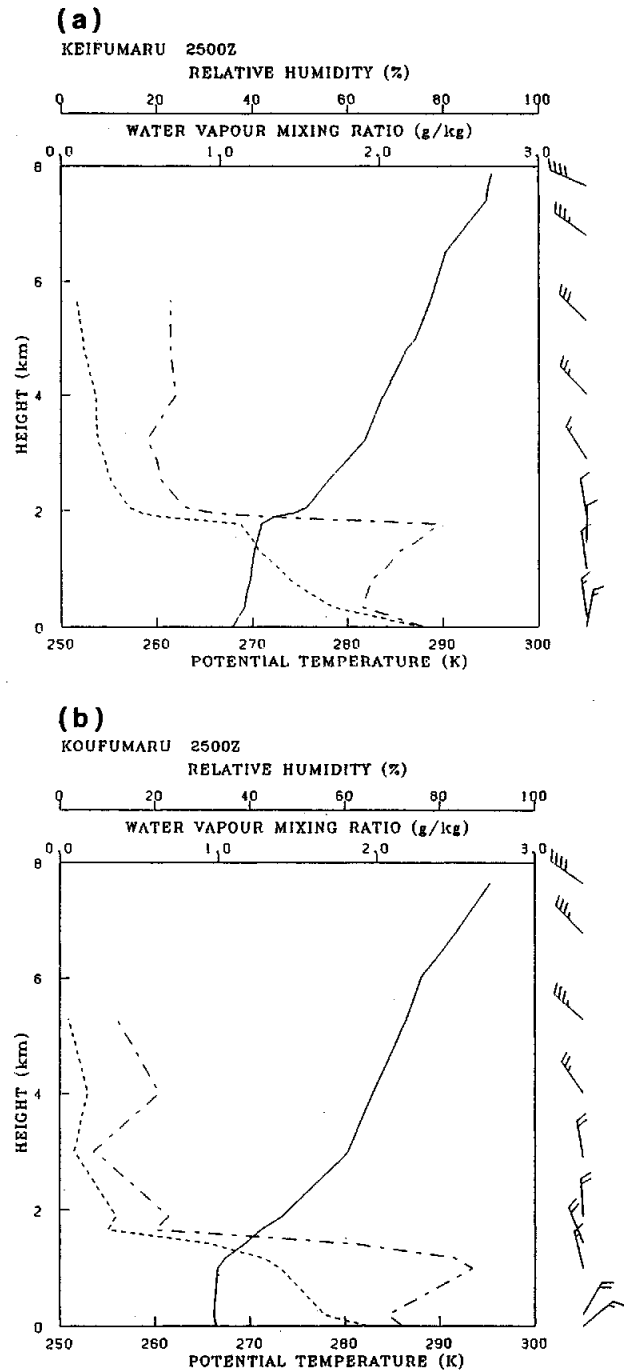


Fig. 6. Soundings at the ships whose positions are shown in Fig. 5. Vertical profile of potential temperature (solid line), relative humidity (dash-dotted line), water vapour mixing ratio (dotted line) and wind (a half barb indicates 5 knots and a full barb 10 knots) at 0900 JST on 25 January 1989. (a) Keifumaru (A in Fig. 5), (b) Kofumaru (B in Fig. 5).

at Kofumaru (-5.0°C , 72%). This indicates that the air mass at Keifumaru traveled over warm water of the Japan Sea much longer than that at Kofumaru

and the air at Keifumaru was modified more than that at Kofumaru.

3. Numerical model

3.1 Model description

We use a 2-dimensional non-hydrostatic elastic model (Satomura, 1989) including the Coriolis force. We set up the calculation domain in the $x-z$ plane, where x and z designate the horizontal (eastward) and the vertical (upward) direction, respectively. The y axis directs northward. Since we assume that the convergence cloud band is two-dimensional, the differentials in the y -direction of all the variables are zero. Time-dependent variables are U , V , W , θ , c , Q_v , Q_c , Q_i , Q_r , Q_s and Q_g , where (U , V , W) are the velocity components in the x , y and z direction respectively; θ the potential temperature deviation from a constant value; π the perturbed Exner function; (Q_v , Q_c , Q_i , Q_r , Q_s and Q_g) the mixing ratios of water vapour, cloud water, cloud ice, rain, snow and graupel, respectively. We use a bulk parameterization of cloud microphysics including both the water phase and the ice phase based on Lin *et al.* (1983), and the production terms of graupel are modified by Ikawa *et al.* (1987). Momentum, heat and moisture fluxes from the surface are calculated by the method of Barker and Baxter (1975) which is based on the Monin-Obukhov similarity theory. The level-2 closure model (Mellor and Yamada, 1974) is used as a diffusion process. We also adopt a fourth-order artificial smoothing in the horizontal direction.

The model atmosphere of 7.6 km height is unequally divided into 20 layers in the vertical direction. The domain is horizontally covered with 600 grid points at an interval of 1 km. In order to confirm that the horizontal grid interval, δx , did not affect the simulated convection, we performed an experiment using $\delta x = 500$ m. Since the results were almost same as those in the case where we adopted $\delta x = 1$ km, we employed 1 km as δx in this study. Concerning a time integration scheme, a time-splitting method similar to Klemp and Wilhelmson (1978) is used in this study: the terms in the momentum and the continuity equations used in our model are split into sound-wave components and remaining terms. The sound-wave components are integrated with a small time step (2 seconds) and the remaining terms are calculated at a large one (10 seconds).

We regard the surface of 0–100 km as a land (the Asian Continent), that of 100–500 km as a sea (the Japan Sea) and that of 500–600 km as land (Hokkaido). Roughness lengths are assumed to be 50 cm on the land and 0.005 cm on the sea. At the bottom boundary, all the time-dependent variables are assumed to be zero except θ and Q_v . At the top boundary, all the time-dependent variables are assumed to be constant and Rayleigh damping is

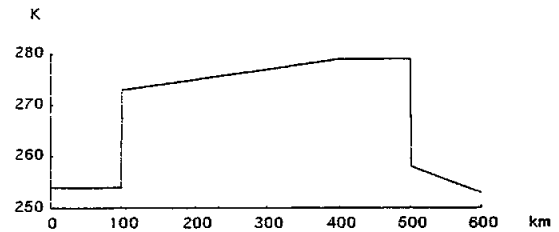


Fig. 7. The lower boundary condition of temperature in numerical experiments.

used above 4 km height to prevent the reflection of waves. As the side boundary conditions of U , we use the radiation condition (Orlanski, 1976) at outflow boundaries and the horizontal gradient is assumed to be zero at inflow boundaries. The horizontal gradients of the other variables are assumed to be zero at both sides.

3.2 Description of the experiments

In the first place, we describe the conditions of Case 1. Figure 7 indicates the bottom boundary condition of temperature. The sea surface temperature is based on THE TEN-DAY MARINE REPORT from 21 to 31 January, 1989 (published by the JMA), and it has a horizontal gradient in the west-east direction. It is noteworthy that the sea surface temperature is 21 K higher than the ground temperature at the coast of Hokkaido. Since the land is covered with snow, the surface humidity is 100% everywhere on both the land and the sea. Initial conditions of potential temperature and humidity in the air are based on the observation at Ternei at 0900 JST on 25 January (Figs. 8a and 8b). A lower layer is stable initially and a mixed layer will be formed over the warm sea as the time integration proceeds. Figures 8c and 8d show initial conditions of U and V , respectively, based on the grid-point data at 43.125°N, 140.625°E (the vicinity of Keifumaru) in GANL (Global Analysis issued by the JMA). It should be noted that the wind in the lower layer is northerly. The orography is excluded in all experiments except one described later. We use Case 1 as a control run.

In Case 2, the sea surface temperature is set to 279 K everywhere to examine the effect of the horizontal gradient of the sea surface temperature on the convergence cloud bands and the wind in the mixed layer.

In Case 3, we use an initial condition $V = 0$ m/s everywhere to examine the effect of V on the convergence cloud bands. The observed V has a gradient in the east-west direction: $V = 0$ m/s at Ternei and $V = -10$ m/s at Keifumaru. We use, however, horizontally constant values as the initial condition of V in order to decrease the parameters affecting the simulated results (the detailed description of this point will be given in the later section). We study the

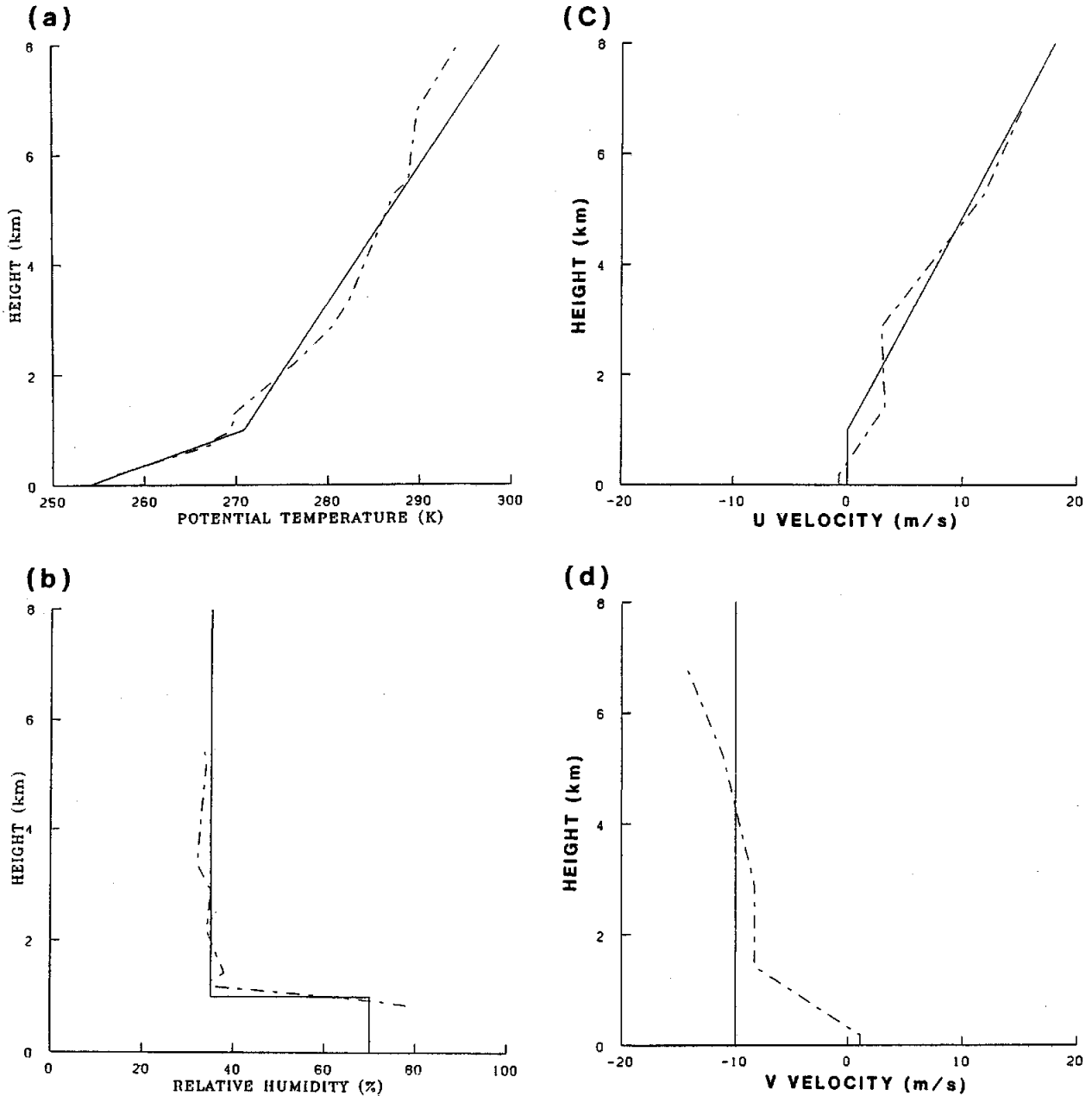


Fig. 8. Profiles of (a) potential temperature, (b) relative humidity, (c) U and (d) V . Solid lines represent the initial condition used in the model. Dash-dotted lines represent the observation at Ternei in (a) and (b), and the grid point data at 43.125°N , 140.625°E (the vicinity of Keifumaru) of the global analysis (GANL) made by the JMA in (c) and (d).

effect of V by comparing the results in Case 1 and Case 3.

In Case 4, the cloud physical processes are neglected (dry model). Since absolute humidity is extremely low when temperature is low, the effect of latent heat might be considered to be small in our case. However, active cumulus observed in the convergence cloud bands are a manifestation of concentrated latent heat release. In order to evaluate the effect of latent heat, we perform the experiment using a dry model and compare the results with those

of Case 1 (moist model).

Four other numerical experiments are performed in order to study the factors which determine the position of EC: (i) the orography is included; (ii) the potential temperature of the ground is increased 10 K from that in Case 1; (iii) the initial condition of U under the height of 1200 m is set to 3 m/s while $U = 0$ m/s in Case 1; and (iv) the horizontally-constant ground surface temperature (258 K) is adopted in Hokkaido.

In each experiment, we divide the time process

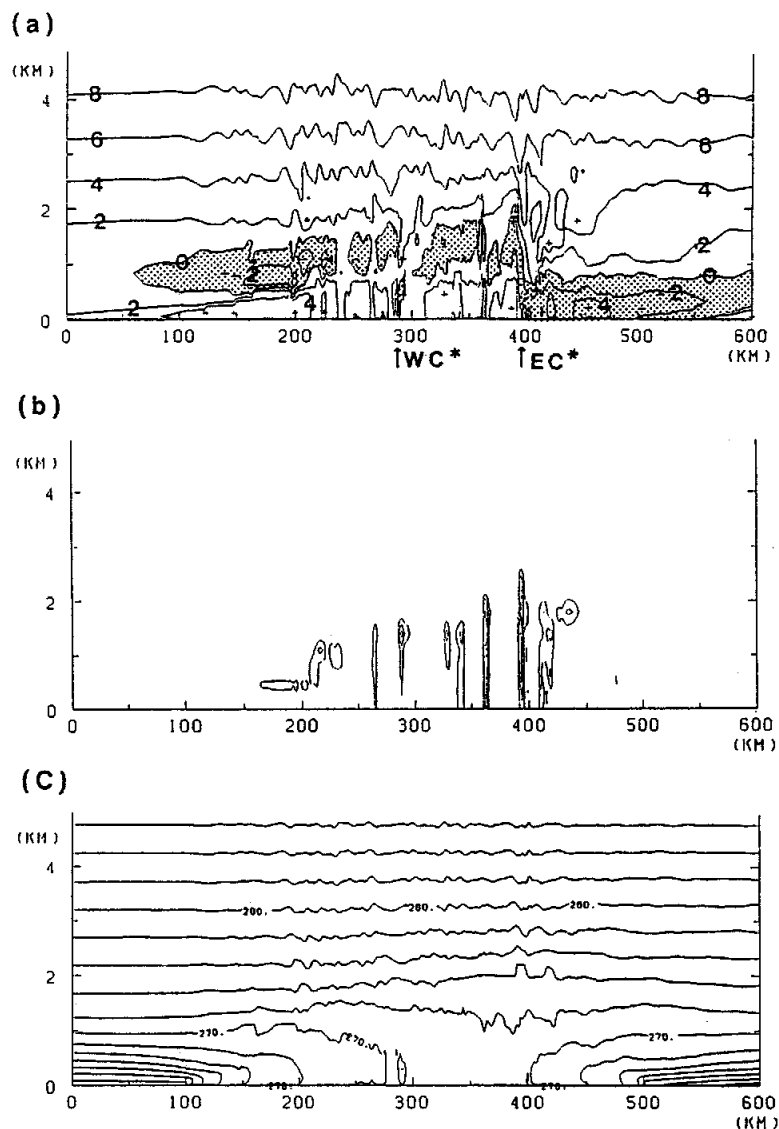


Fig. 9. Vertical cross sections of (a) U with the contour interval of 2 m/s (shaded areas are negative values), (b) $(Q_c + Q_i + Q_r + Q_s + Q_g)$ with the contour interval of 0.2 g/kg and (c) potential temperature with the contour interval of 2 K at $t=16$ h in Case 1.

into two stages for an economical reason. In the first stage, during the time when the air is saturated very little, we perform the integration without using the parameterization of cloud microphysics. In the second stage, we perform the integration with all the processes. The total time of the two stages is set to be 16 hours in each experiment, since the depth of mixed layer and the position of EC is almost steady at that time. We also completed the time integration with all the processes from the beginning in Case 1, and we confirmed that the results scarcely differed from those presented in this paper.

4. Results of numerical experiments

4.1 Control run

Figure 9a is a vertical cross section of U at $t=16$ h (16 hours after the initiation of the model) in Case 1. It shows that land breeze is blowing easterly from

Hokkaido and reaches the vicinity of 400 km (100 km off the west coast of Hokkaido). A westerly wind is blowing to the west of that point. A strong upward wind is present at that point owing to the convergence of the easterly wind and the westerly wind in the lower layer. The position of EC* (hereafter we mark the simulated EC and WC with *) is almost the same as that observed by the radar and GMS. Figure 9b is a vertical cross section of condensed water plus coagulated water ($Q_c + Q_i + Q_r + Q_s + Q_g$) at $t=16$ h. The maximum value (1 g/kg) of ($Q_c + Q_i + Q_r + Q_s + Q_g$) is found at the convergence zone: Q_c , Q_s , Q_g are about 0.4, 0.2 and 0.5 g/kg, respectively; Q_i and Q_r are negligible compared to the others. The upper boundary of the layer including liquid or solid water is highest there. Figure 9c is a vertical cross section of potential temperature at $t=16$ h. The depth of the mixed layer increases

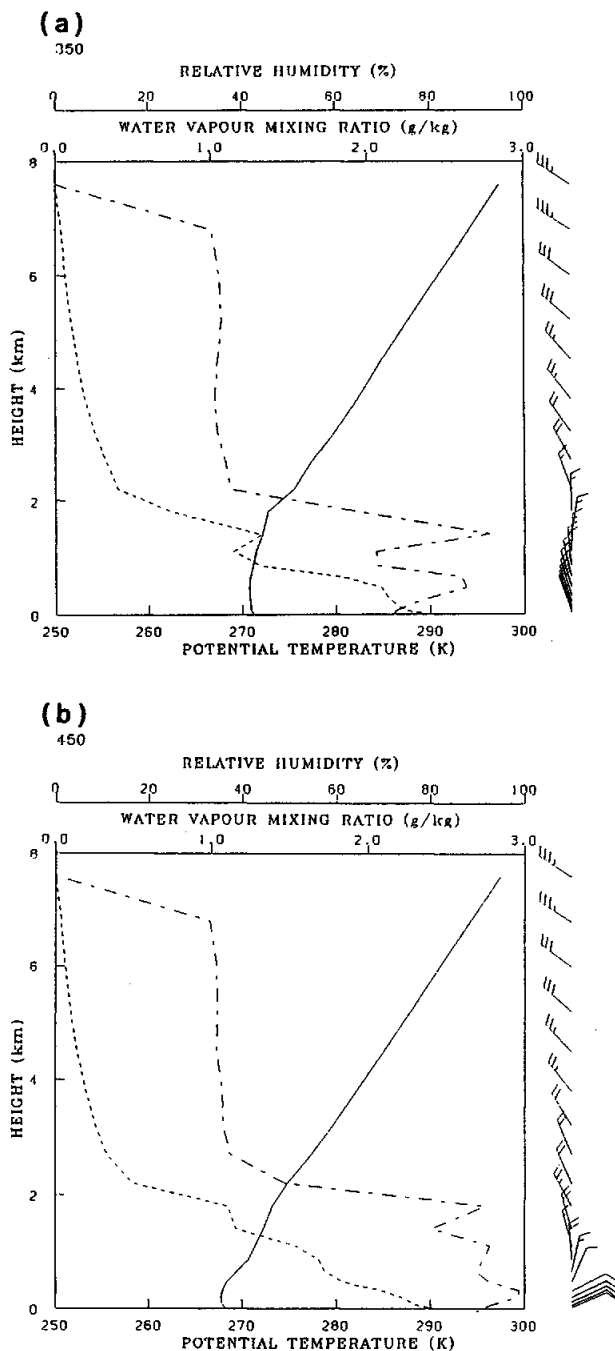


Fig. 10. Calculated vertical profiles of potential temperature (solid line), relative humidity (dash-dotted line), water vapour mixing ratio (dotted line) and wind (a half barb indicates 5 knots and full barb 10 knots) at $t=16$ h in Case 1. (a) at 350 km (corresponding to the position of Keifumaruru), (b) at 450 km (corresponding to the position of Kofumaruru).

with a distance from each coast. It is deepest (about 2 km) in the vicinity of EC*.

Figure 10a shows vertical profiles of potential temperature, relative humidity and water vapour

mixing ratio at 350 km (50 km west of EC*) corresponding to the position of Keifumaruru. Both calculated potential temperature and water vapour mixing ratio are a little larger than the observed values in the mixed layer. The sudden changes of potential temperature and water vapour mixing ratio at the upper boundary of the mixed layer are expressed well by the simulation, and the depth of the mixed layer is almost the same as that observed. On the other hand, the depth of mixed layer (about 500 m) is much shallower than that observed (about 1200 m) at 450 km (50 km east of EC*) which corresponds to the point of Kofumaruru (Fig. 10b).

Figure 9a also indicates a small region of the easterly wind in the lower layer and weak convergence around 280 km. This convergence, WC*, is located about 100 km east of the observed WC, but we will indicate in section 5 that WC* corresponds to WC by comparing the results in Case 1 with those in Case 2 and Case 3. The cold air from the continent reaches the west side of WC* and there is an ascending current at WC*. Weak convection is also found in the same region. The easterly wind in the vicinity of WC* is induced by this vertical circulation. Judging from the above situation, the cold air from the Asian Continent does not reach the west side of EC*.

4.2 The effect of the sea surface temperature gradient

Figure 11a shows the westerly wind, U , at $t=16$ h in Case 2. It is found that EC* is almost the same position as that in Case 1 but it becomes weak. It is also found that there is another strong convergence (WC*) at 220 km (120 km east of the coast of the Asian Continent). The easterly wind region on the east side of WC* is larger and stronger than that in Case 1. The wind direction is not uniformly west between EC* and WC* in Case 2, while the westerly wind is blowing in the same region as in Case 1.

4.3 The effect of initial V

The experiment with the initial value of $V=0$ m/s is performed in Case 3 to see the effect of initial V . Figure 11b shows contours of U at $t=16$ h in Case 3. A strong convergence as in Case 1 is not found off the west coast of Hokkaido. On the other hand, there is a strong convergence compared with that in Case 1 at 160 km (60 km off the coast of the Asian Continent), and it is snowing there (not shown). The position of WC* is almost the same as that observed. The depth of mixed layer over the whole region is much shallower than that in Case 1 because heat and moisture fluxes from the surface are weak owing to the low wind velocity in the lowest layer. A region of easterly wind on the east side of WC* is also found in this case.

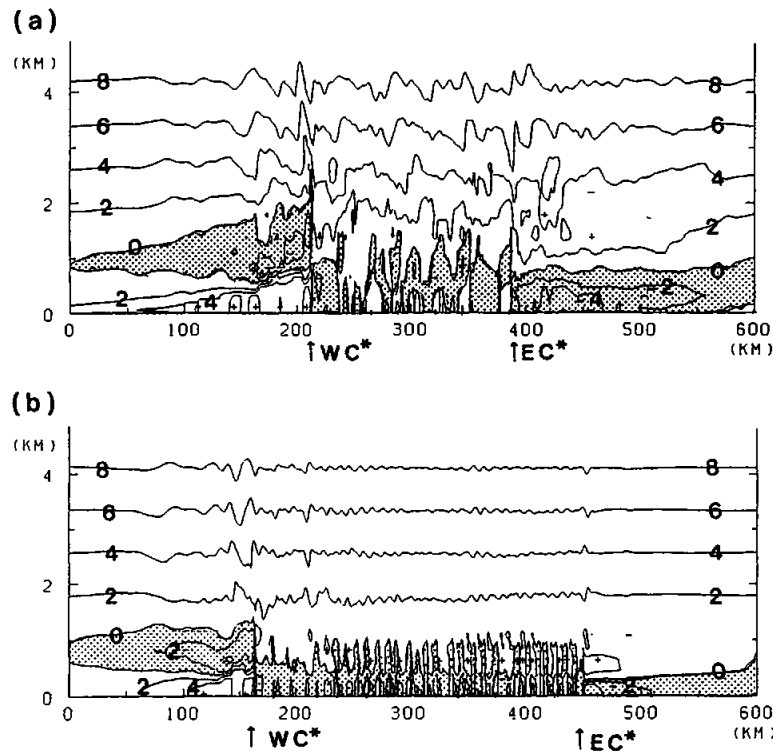


Fig. 11. Vertical cross sections of U with the contour interval of 2 m/s at $t=16$ h (shade areas are negative values): (a) Case 2, the sea surface temperature is 279 K everywhere, (b) Case 3, $V=0$ m/s.

4.4 The effect of latent heat

Average sensible heat flux from the sea (100 km~500 km) and latent heat release estimated from the precipitation over the sea at $t=16$ h in Case 1 are 1.9×10^5 J/m²/hour and 1.8×10^5 J/m²/hour, respectively. Thus, the effect of latent heat is an important factor in the development of the mixed layer and the convergence cloud band. To show this effect more directly, we performed the experiment excluding the cloud physical processes. Figures 12a and 12b are vertical cross sections of U and potential temperature at $t=16$ h, respectively. The position of EC^* shifts only 20 km to the east, but the mixed layer does not develop well: the depth of the mixed layer around the center of the domain is about 1 km. Therefore, we conclude that the effect of latent heat on the convergence cloud band is large.

4.5 The position of EC^*

The following four experiments are performed to study the factors which determine the position of EC^* . When the orography is included (Fig. 13a), the easterly wind ($U \approx -10$ m/s) on the slope of the mountain in Hokkaido (from 500 km to 530 km) is much stronger than the wind at the same position in Case 1 ($U \approx -3$ m/s). The position of EC^* , however, shifts to the west only a little because a hydraulic jump occurs at the coast and the wind becomes weak over the sea. When the ground temperature of Hokkaido is increased 10 K from that in Case 1

(Fig. 13b), the position of EC^* shifts to 440 km (60 km west to the coast), while the position is 400 km (100 km off the west coast of Hokkaido) in Case 1. When the initial condition of U below 1200 m is 3 m/s (Fig. 13c), the position of EC^* is located about 60 km east of that in Case 1: 460 km (40 km west of the coast). When the ground surface temperature of Hokkaido is constant horizontally, the result (not shown) is almost the same as that in Case 1. Therefore, the difference between the sea and the ground surface temperature at the coast of Hokkaido is an important factor to determine the position of EC^* , but the horizontal gradient of the ground temperature of Hokkaido is far less important. A westerly wind in the lower layer affects the position seriously. The orographic effect of Hokkaido on EC is small in this case.

5. Discussion

Generally, cold air blows out from both the Asian Continent and Hokkaido, and is gradually modified by the accumulation of sensible heat and latent heat. Since the trajectory of the air can not be expressed precisely in a 2-dimensional model, the amount of heat and water vapour supplied from the warm sea can not be calculated exactly. We, however, consider that two dimensional models can represent the modification of air due to the heat and moisture supply from the warm sea surface approximately if the following two conditions are satisfied: i) the models

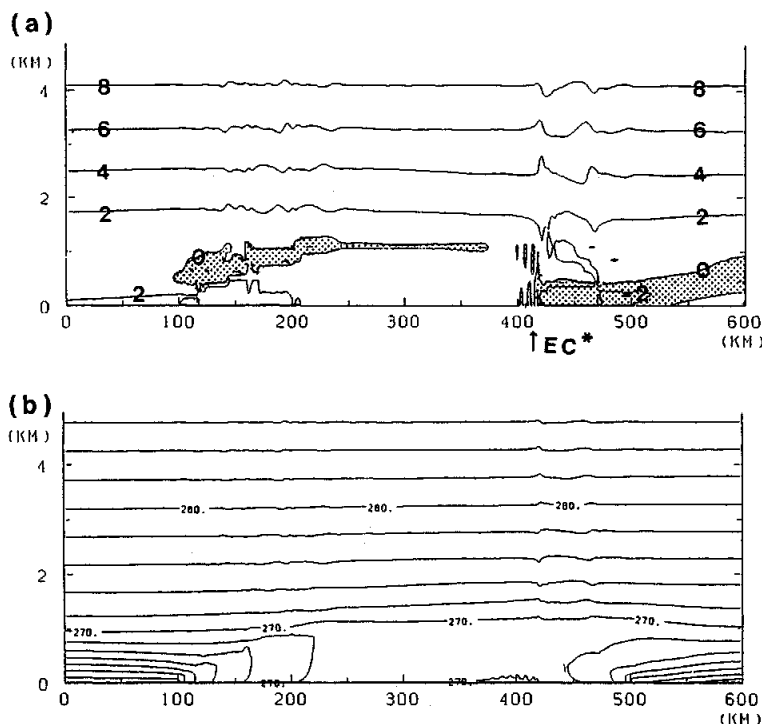


Fig. 12. Vertical cross sections of (a) U with contour interval of 2 m/s (shaded areas are negative values) and (b) potential temperature with the contour interval of 2 K at $t=16$ h in Case 4 (dry model).

simulate the wind velocity well, ii) the y -differentials of variables are nearly equal to zero in the real atmosphere. The satisfaction of the condition i) guarantees a representative flux from the sea, because the flux increases with the wind velocity. If the condition ii) is satisfied in addition to i), the fetch is evaluated almost correctly in the model. In our case, the above two conditions are roughly satisfied near the coast of the Asian Continent. Therefore, the model can approximately include the process of modification of the air mass around WC^* . Near the coast of Hokkaido, on the other hand, condition ii) is not satisfied because of complexity of the coast line: there are bays, peninsulas and promontories. Thus, the depth of mixed layer at 450 km in Case 1 is not well simulated.

Since there is a small region of the easterly wind on the east side of WC^* in Case 1, the cold air from the Asian Continent stops at WC^* . Therefore, the cause of the westerly wind between EC^* and WC^* is not obvious. Two forces are supposed to cause this westerly wind: the pressure gradient force and the Coriolis force. The pressure gradient force is made from the gradient of total diabatic heating caused by the gradient of the sea surface temperature. On the other hand, the Coriolis force working on the ageostrophic wind accelerates the westerly wind: the northward ageostrophic wind results from decelerating the initial geostrophic wind $V = -10$ m/s mainly owing to the dissipation process in the mixed layer. In order to examine which force is more important

in Case 1, we sum up the terms of the Coriolis force $f(V - V_0)$ and the pressure gradient force $-C_p(\theta + \theta)\partial\pi/\partial x$, respectively in the U -equation between EC^* and WC^* in the layers of the westerly wind, where f is the Coriolis parameter, V_0 is the initial value of V and θ is the potential temperature of the basic state. The result shows that the pressure gradient force is about two times as large as the Coriolis force. In addition, the wind directions between EC^* and WC^* in Case 2 are indefinite. For the above reasons, we conclude that the weak westerly wind between EC^* and WC^* in Case 1 is mainly formed by the horizontal gradient of the sea surface temperature.

The positions of WC^* in Case 2 and in Case 3 are 60 km and 120 km west of that in Case 1, respectively. We consider the reason for the difference in position as follows: In Case 1, the Coriolis force working on the ageostrophic wind and the pressure gradient force due to the gradient of the sea surface temperature accelerate the westerly wind around WC^* for the same reason that the westerly wind is blowing between EC^* and WC^* . In Case 2, the sea surface temperature has no horizontal gradient, while the gradient in Case 1 is 6 K/300 km. This means that the westerly wind acceleration around WC^* due to the gradient of the sea surface temperature is absent in Case 2. On the other hand, the difference of the surface temperature between the Asian Continent and the sea in Case 2 is larger than that in Case 1. This temperature difference accelerates

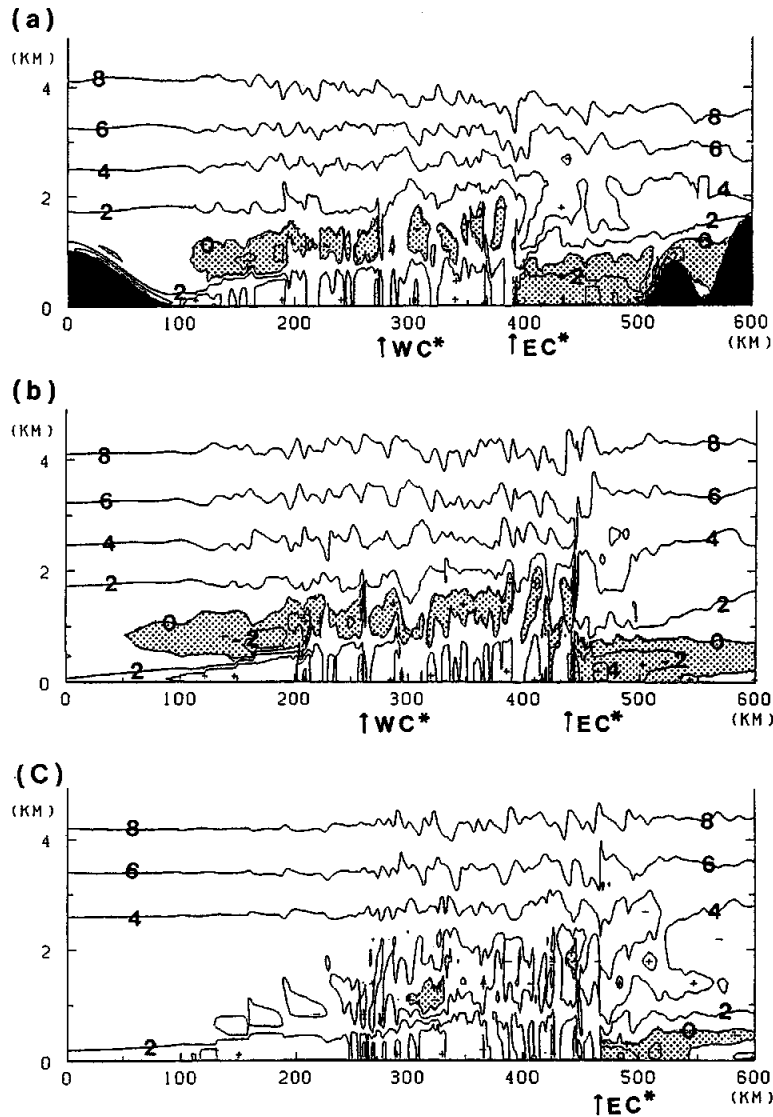


Fig. 13. Vertical cross sections of U with the contour interval of 2 m/s (shade areas are negative values) at $t=16$ h: (a) the orography is included, (b) the potential temperature of the ground is increased 10 K from that in Case 1, (c) the initial condition of U under the height of 1200 m is set to 3 m/s.

ates the westerly wind around WC^* . Looking into the result that WC^* in Case 2 is located at 60 km west of the position in Case 1, the gradient of the sea surface temperature influences the position of WC^* more than the sea-land temperature difference. In Case 3, not only the Coriolis force but also the heat and moisture flux from the sea surface differ from those in Case 1, because the wind is weaker than that in Case 1. This suggests that both the Coriolis force and the pressure gradient force strongly affect the difference in position of WC^* between Case 1 and Case 3.

In Case 1, the position of EC is simulated well, but the position of WC^* does not agree with the observation. On the other hand, the position of WC^* in Case 3 is almost the same as that observed, but EC^* is weak and the position of EC^* is shifted to 450 km (50 km off the coast of Hokkaido). The initial

wind is determined from the data of GANL in the vicinity of Keifumaru in Case 1, while the observed wind at Ternei was weak in the lower layer because there was an anticyclone over Primorskii. The initial wind in Case 3 is close to the wind at Ternei. Each convergence (EC and WC) can be well simulated in the experiment whose initial wind is close to that observed around the convergence. Thus, we consider that EC^* and WC^* correspond to EC and WC , respectively. If we use the initial value of V close to that in the real atmosphere, we might be able to simulate the positions and the strength of both EC and WC well in one experiment. But this is not our objective. Further, the initial value of V stated above would have a vertical gradient, and it introduces $\partial\theta/\partial x \neq 0$ in the initial condition from the thermal wind relation. The increase in number of parameters ($\partial v/\partial z$ or $\partial\theta/\partial x$, $\partial v/\partial x$) complicates

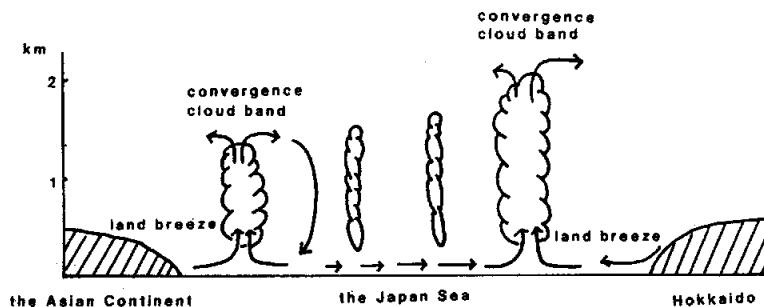


Fig. 14. Schematic structure of the two convergence band clouds which appeared over the northern part of the Japan Sea on 24 to 25 January 1989.

interpretation of the results.

The heights of the cloud tops at EC* in Case 1 and WC* in Case 3 are 2500 m and 1500 m, respectively. On the other hand, the heights of the cloud tops at EC and WC are estimated from the minimum brightness temperature obtained from GMS and the temperature profile at Keifumar, and they are 1800 m and 1200 m, respectively. The estimated heights are considered to have errors of several hundred meters because the vertical distributions of temperature at WC and EC were different from that at Keifumar. The real heights of the cloud tops should be higher than the estimated ones because we used the sounding data at Keifumar, where convection is not as active as at EC and WC, to estimate the height. Hence, the heights of cloud tops at EC and WC are only approximately simulated.

The model used in this study is 2-dimensional. Therefore, there are many restrictions: convection in a plane perpendicular to the east-west axis can not be represented; the modification of air can not be treated precisely owing to the limited representation of flowing distance; and a north-south component of temperature advection can not be included. Therefore, a 3-dimensional model is necessary to settle those problems. The process of the radiational cooling also has to be included because the surface temperature of Hokkaido is an important factor in the formation of EC. If the model represents a convergence cloud band more accurately after the modifications stated above, the prediction of its time, location and quantity of heavy snowfall by the model will be useful to reduce or prevent the disaster. These predictions are, however, left for future work.

6. Summary

We performed numerical experiments of two convergence cloud bands and compared the results with observations on 25 January 1989. The convergence cloud bands were observed about 100 km off the west coast of Hokkaido and 70~80 km off the east coast of the Asian Continent by GMS on that day. In Case 1 (control run), EC was simulated at almost the same position. Cold air blew out from both

the Asian Continent and Hokkaido, and was gradually modified by the accumulation of sensible heat and latent heat. The mixed layer was deepest at EC*. The mixed layer at 450 km was considerably shallower than that observed at Kofumar. On the other hand, at 350 km, not only the depth of the mixed layer but also the profiles of the calculated potential temperature and the water vapour mixing ratio agreed well with those observed at Keifumar.

There was a small region of easterly wind on the east side of WC* in Case 1. Therefore, the cold air from the Asian Continent stopped at WC* and did not reach the west side of EC*. There was, however, a westerly wind region in the lower layer between EC* and WC*. The total diabatic heating from the sea surface that had a horizontal temperature gradient produced the pressure gradient. Because this pressure gradient force was larger than the Coriolis force in the horizontally averaged U -equation, it caused the westerly wind between EC* and WC*. Thus, we concluded that the westerly wind in this case was caused not by the monsoon from the continent but by the horizontal gradient of the sea surface temperature.

In the case where the initial value of V was 0 m/s (this situation was similar to Ternei's one), the calculated position of WC* was almost the same as that observed. The comparison between Cases 1, 2 and 3 suggested that the Coriolis force and the pressure gradient force strongly affected the difference in position of WC*.

In the case of the dry model, the position of EC* shifted a little to the east, but convection was very weak and the mixed layer was shallow. Therefore, the water vapour was necessary for convection to develop fully, as was observed.

Four other experiments were performed to study the factors which determined the position of EC*. We found that the difference between the sea and the land surface potential temperature at the coast of Hokkaido was an important factor to determine the position of EC* but the horizontal gradient of the ground surface temperature of Hokkaido was not. Wind U in the lower layer affected the position seri-

ously while the orographic effect on EC* was small.

Figure 14 shows the schematic structure of the two convergence cloud bands obtained from the observation and the numerical experiments. The cold air is blowing from the Asian Continent and stops at 70~80 km off the east coast of the continent. There are convergence and convection at that point. The easterly wind is blowing on the east side of the convergence owing to the secondary circulation of the ascending current. The land breeze is also blowing from Hokkaido and a convergence cloud band is formed about 100 km off the coast. The westerly wind between two convergence cloud bands is caused by the sea surface temperature gradient.

Acknowledgments

The authors would like to thank the Marine Meteorological Division of the JMA, the Hakodate Marine Meteorological Observatory and the Sapporo District Meteorological Observatory for offering the observational data. The authors wish to extend their gratitude to H. Okubo of the JMA for his valuable discussions and M. Ikawa for helpful suggestions on cloud physical parameterization.

References

- Ballentine, R.J., 1982: Numerical simulation of land-breeze induced snowbands along the western shore of Lake Michigan. *Mon. Wea. Rev.*, **110**, 1544-1553.
- Barker, E.H. and T.L. Baxter, 1975: A note on the computation of atmospheric surface layer fluxes for use in numerical modeling. *J. Appl. Meteor.*, **14**, 620-622.
- Fujiyoshi, Y., K. Tsuboki, H. Konishi and G. Wakahama, 1988: Doppler radar observation of convergence band cloud formed on the west coast of Hokkaido Island (I): warm frontal type. *Tenki*, **35**, 427-439 (in Japanese).
- Hjelmfelt, M.R. and R.R. Braham, Jr., 1983: Numerical simulation of the airflow over Lake Michigan for a major lake-effect snow event. *Mon. Wea. Rev.*, **111**, 205-219.
- Ikawa, M., H. Sakakibara, M. Ishihara and Z. Yanagisawa, 1987: 2-dimensional simulation of the convective snow band observed over the Japan Sea:— the structure and time evolution of the organized multicellular convection—*J. Meteor. Soc. Japan*, **65**, 605-633.
- Klemp, J.B. and R.B. Wilhelmson, 1978: The simulation of three-dimensional convective storm dynamics. *J. Atmos. Sci.*, **35**, 1070-1096.
- Lin, Y., R.D. Farley and H.D. Orville, 1983: Bulk parameterization of the snow field in a cloud model. *J. Climate Appl. Meteor.*, **22**, 1065-1092.
- Mellor, G.L. and T. Yamada, 1974: A hierarchy of turbulence closure models for planetary boundary layers. *J. Atmos. Soc.*, **31**, 1791-1806.
- Muramatsu, T., S. Ogura and N. Kobayashi, 1975: The heavy snow-fall arisen from small scale cyclone on the west cost of Hokkaido Island. *Tenki*, **22**, 369-379 (in Japanese).
- Nagata, M. and M. Ikawa, 1988: Numerical experiments of the convergent cloud band over the Japan Sea. *Tenki*, **35**, 151-155 (in Japanese).
- Okabayashi, T., 1969a: Photograph of heavy snowfall on Japan Seaside on Jan. 2. 1969, taken by ESSA. *Tenki*, **16**, 79-80 (in Japanese).
- Okabayashi, T., 1969b: On the convergent band cloud appeared on the satellite picture and small scale low. *Tenki*, **16**, 371-372 (in Japanese).
- Okabayashi, T. and M. Satomi, 1971: A study on the snowfall and its original clouds by meteorological radar and satellite (part I). *Tenki*, **18**, 573-581 (in Japanese).
- Orlanski, I., 1976: A simple boundary condition for unbounded hyperbolic flows. *J. Comput. Phys.*, **21**, 251-269.
- Saito, M., F. Jinoka, H. Matsuda, M. Satomi and R. Obana, 1968: Radar analysis of the snowfalls in the vicinity of the Ishikari Bay in Hokkaido. *Tenki*, **15**, 42-50 (in Japanese).
- Sasaki, H. and S. Deguti, 1988: Numerical experiments of the convergent band formed off the western coast of Hokkaido in winter. *Tenki*, **35**, 723-729 (in Japanese).
- Satomura, T., 1989: Compressible flow simulation on numerically generated grids. *J. Meteor. Soc. Japan*, **67**, 473-482.
- Tsuboki, K., Y. Fujiyoshi and G. Wakahama 1989: Doppler radar observation of convergence band cloud formed on the west coast of Hokkaido Island. II: cold frontal type. *J. Meteor. Soc. Japan*, **67**, 985-999.

日本海北部に形成される収束雲の数値実験

佐々木秀孝・里村雄彦

(気象研究所応用気象研究部)

日本海北部に発生した二本の収束雲のシミュレーションを二次元非静水圧モデルで行い、気象庁の行った特別観測の結果と比較した。モデルは、水平方向に 600 km の計算領域を持ちアジア大陸・日本海・北海道を含んでいる。

北海道の西岸沖 100 km と、アジア大陸東岸沖数十 km に収束雲をシミュレートした。また、アジア大陸から流れてきた寒気は、西側の収束雲の所で止まり、北海道からの陸風は東の収束雲の所で止まっていることが分かった。

風の初期値、海面・陸面の表面温度、潜熱の解放、それに地形の影響などが、それらの収束雲にどのような影響を与えるかを調べるためにさらにいくつかの実験を行った。その結果、二本の収束雲の間に吹いている西風は、海面水温の水平傾度から生じた気圧傾度圧によって出来ることが分かった。潜熱は、対流が十分発達するのに必要である。また、北海道の海岸における海陸の温度差、及び下層における風の初期値は、東側の収束雲の位置を決定するには重要な要素であることが分かった。